Transport in Nanoporous Carbon Membranes: Experiments and Analysis

Madhav Acharya and Henry C. Foley
Center for Catalytic Science and Technology, Dept. of Chemical Engineering, University of Delaware, Newark, DE 19716

Single-component permeances of six gases were measured on three different supported nanoporous carbon membranes prepared by spray coating and pyrolysis of poly(furfuryl alcohol) on porous stainless-steel disks. Global activation energies were regressed from data collected as a function of temperature. Permeances and global activation energies were correlated to molecular size, assuming that entropic affects dominated the transport. The permeance was best correlated to the minimum projected area of the molecule computed from first principles. The free-energy barriers to transport within the membranes were derived from the temperature dependence of the permeance data, after accounting for porosity differences between the membranes and differences in molecular adsorption. Using transition-state theory and an entropic model derived, the free energy, enthalpy, and entropic barriers to transport within the membrane were examined as a function of molecular size. Computed on the basis of size, the entropic component of this barrier did not account for the large differences in the transition-state free energies. However, when these entropic barrier values were used to compute the enthalpic portion of the barrier free energies, the minimum projected area of each molecule correlated strongly. Furthermore, these enthalpic components of the barriers were fitted nicely by the Everett-Powl mean field potential, using only the pore size as the adjustable parameter. These results shed light on the underlying mechanism by which shape-selective transport takes place in the NPC membranes and small molecules are separated.

Introduction

Ceramic membrane technology is being developed rapidly for a variety of gas separations. Since membranes can be more energy efficient, and therefore more economical than other methods for gas separation, considerable research is underway to find new highly selective membrane materials. One prominent example is that of the Surface-Selective Flow (SSF) membrane, developed by Air Products and Chemicals. This technology has been commercialized and is able to produce enriched hydrogen streams at high pressure from mixed hydrocarbon and hydrogen feeds (Rao and Sircar, 1993, 1996; Parrillo et al., 1997; Rao et al. 1992). We have shown (Acharya et al., 1997; Acharya and Foley, 1999; Acharya, 1999; Petkov et al., 1999) that nanoporous carbon molecular sieve membranes also can be prepared with very high size and shape selectivity. This offers the opportunity to extend the range of application of carbon membranes beyond that of surface-selective flow alone. That nanoporous carbon molecular sieves with pore sizes less than 5 Å can separate nitrogen from oxygen has been known for some time, and is the basis for nitrogen pressure swing adsorption (NPSA) (Yang, 1987; Ruthven, 1984). This separation, done over packed beds of nanoporous carbon, is considered to be based upon the kinetics of diffusion rather than on the thermodynamics of adsorption (Juntgen et al., 1981; LaCava et al., 1989; Suzuki, 1990). Entropic effects at the narrowest points of the complex pore networks of nanoporous carbons (NPC) may provide the nec-

Correspondence concerning this article should be addressed to H. C. Foley.
Current address of M. Acharya: Mobil Technology Company, Paulsboro, NJ 08066.

essary discrimination between oxygen and nitrogen (Singh and Koros, 1996; Kane et al., 1996).

The relationship between transport and molecular size for NPC and other materials is one that presents an ongoing challenge. Several authors have approached this problem empirically by plotting the permeance for a given molecule against its characteristic dimension, typically the kinetic diameter (Shelekhin et al., 1995; Kasakabe et al., 1998). Although valuable in a global sense, since data of this kind allow one to compare the behaviors of different membrane materials, there are complications in its interpretation. First, the permeance is a convolution of molecular adsorption and diffusive transport. Second, it is not clear that the appropriate size of the molecule is the kinetic diameter when one is considering transport in nanopores that are commensurate in size with the molecule within it. This issue has been pointed out by the group at Air Products and Chemicals, Inc. They concluded that when working with nanoporous carbons for air separations, the van der Waals diameters were a better measure of molecular dimension than were kinetic diameters, though the latter are more typically used (Moyer et al., 1994).

Bulk NPC employed in NPSA consists of a network of pores with a layer at the external surface of the particles, which act as ''gate-keepers'' to the underlying pores and which are responsible for sieving. The importance of this gate-keeping layer is most vividly demonstrated in the work from Air Products (Cabrera et al., 1993; Braymer et al., 1995) and Verma and Walker (1992). Both groups have shown that the rates of transport of small molecules through carbon molecular sieves can be differentially attenuated. The hypothesis is that by cracking hydrocarbons over NPC, carbon is deposited that creates narrow slit-shaped pore mouths. The critical slitlike geometry in NPC, and the attribution to these pores of highest resistance to the selectivity in the transport, was first proposed by Walker and coworkers on the basis of careful adsorption experiments using differently shaped and sized molecules (Lamond et al., 1965). Walker went so far as to envision the pore structure to be one consisting of large dimension (>5 Å), low resistance galleries connected by very narrow, high resistance slitlike entrances and exits. Recent work using STM (Rao and Sircar, 1996) and HRTEM (Kane et al., 1996; Petkov et al., 1999) has lent support to this intuitive view of NPC structure. Chemically and physically constrained models of these materials (Acharya et al., 1999) also indicate that Walker's intuitive structural insights were largely correct. Walker went on to suggest that transition state theory could be applied to modeling the diffusivity in such a pore network, whether it was a nanoporous carbon or a zeolite (Walker et al., 1965). In this way, he anticipated much of the work devoted to the simulation and modeling of transport in zeolites that emerged from the middle 1980s through the early 1990s.

Chihara and coworkers made a detailed study of nanoporous carbon pore-size distribution (Chihara et al., 1978a) and molecular transport within these materials (Horvath and Kawazoe, 1983; Chihara et al., 1978b; Kawazoe et al., 1974, 1978). Their analysis of nonoscale molecular transport systems took an abstract view of the process; they idealized the motion of a molecule within an NPC pore to that of a particle jumping between potential wells. They used a sinusoidal field to model the potential within the pore and derived the following expression for the diffusivity:

$$D = C_a^2 \left(\frac{M^*}{M} \right) \left(\frac{V_o}{2ma^2} \right)^{1/2} e^{(-E_{a,\mathrm{diff}}/RT)}. \qquad (1)$$

The preexponential factor can be written as D_{C0}; C_a is a constant, a is the jump distance between two active sites, m is the molecular weight, V_0 is the height of the potential barrier between sites, and M^*/M is a constant related to the pore structure. The predicted values for D_{C0} matched the experimental data well for monoatomic gases such as Xe, Kr, and Ar, but were not accurate for hydrocarbons other than methane.

By the early 1990s, the consensus among technologists involved in PSA recovery of nitrogen from air was that nanoporous carbon molecular sieves separated oxygen from nitrogen on the basis of a minute difference in size (~ 0.2 Å); furthermore, this required a pore dimension close to 4 Å (Gaffney, 1996; Armor, 1995). Recently, and in keeping with this notion, Singh and Koros (1996) analyzed the high rate of oxygen over nitrogen transport in nanoporous carbons in terms of a difference in the entropic barriers posed by the pore entrance to the two differently sized molecules. Using the partition functions for both, and an assumed pore entrance dimension of 3.8 Å, they obtained good agreement with experimental data on zeolites and carbon molecular sieves. Ford and Glandt (1995) simulated the penetration probability of hard spheres through a slit-shaped pore employing molecular dynamics. The simulation results were fit to a sixth-order polynomial of the ratio of the molecule to the pore size, thereby once again placing the emphasis on statistical geometric effects at the pore entrance.

In this article, we examine the transport behavior of a set of small molecules in a thin layer of nanoporous carbon molecular sieve derived from polyfurfuryl alcohol in the form of a membrane supported on stainless steel. This builds on our earlier report, in which we described these materials for the first time (Acharya et al., 1997). We show that for these molecules, the permeance of the molecules is best correlated with their projected area computed as the product of their ultimate and penultimate minimum dimensions. Then we go on to analyze the permeance data by separating the adsorption from the transport effects in a classic fashion. In keeping with the original ideas of Walker (1965) and the more recent entropic arguments of Glandt (1995) and Koros (1996), we consider the highest resistance to diffusion through these materials to be located within the very narrowest constrictions that separate large low resistance galleries. If the membrane is to function as a molecular sieve, which these materials do, then all flow must be limited by transport through these points of highest resistance. Any lower-resistance paths provide a diffusive shunt and low selectivity, which is no better than that derived on the basis of Knudsen transport. The molecule must have adequate energy to penetrate the barrier at the constriction, otherwise it returns to the original gallery from which it started. Hence, a transition-state theoretic approach is taken to analyze the free energy of this transition. An analytical model is presented for the entropic effects in terms of the diminution of molecular free volume in going to the transition state. From the model values and the experimental free

energies of transition, we can compute the transition-state enthalpies for each molecule. These values lie between 0 and 12 kcal/mol and are in good agreement with values observed in similar materials, for the same and similar molecules. Finally, in order to ascertain in another way if the range and magnitude of the transition-state enthalpy values is reasonable, the Everett–Powl mean field potential function (EP-MFP) for the energy of a molecule trapped between two graphene sheets was computed. We compared this computed value to the corresponding transition-state enthalpy derived from the experimental data. After adjusting only the pore size (4.6 Å) in the potential function, we found that the computed potential energies agreed well with the experimentally transition-state enthalpies. This pore-size value of 4.6 Å is in good agreement with previous measures of the pore sizes in these NPC materials, and is consistent with their high selectivities. It is also close to, and hence self-consistent with, the assumed value for the mean of the pore-size distribution (4.0 Å) used to compute the entropy.

Experimental Section

Rise-time experiment

Spray-coated membranes were synthesized at 400, 500 and 600°C, based on a method described elsewhere (Acharya, 1999). These will be referred to as membrane A, B, and C in the remainder of the article. Gas permeabilities through these membranes were measured using a rise-time experiment adapted from O'Brien et al. (1986). The apparatus consisted of a gas delivery system connected to a membrane module (containing a retentate and a permeate chamber, as shown in Figure 1), a vacuum pump attached to the permeate side of the module, pressure transducers on either side of the membrane, and two-way valves on the retentate and permeate side of the module. The membrane to be tested was sealed tightly between Viton gaskets in the module. Prior to introduction of the probe gas, both sides of the module were evacuated to 1 torr or less while heating to 40°C to remove any adsorbed molecules from the surface. After the module was cooled to ambient temperature, the two-way valve leading to the vacuum pump was closed and the probe gas was introduced on the retentate side of the membrane. Using a bypass line, the gas also was introduced on the permeate side of the module, and the pressure was raised up to slightly above atmospheric conditions. At this time, the vacuum pump was bypassed and the valve on the permeate side of the membrane was opened. Thus, a continuous gas flux through the membrane was established between the high-pressure and low-pressure sides. The retentate-side pressure of the gas was adjusted by using a small needle valve to produce a bleed stream.

To measure the permeability of the probe gas, the permeate-side valve was closed, as a result of which the pressure of the gas increased on the permeate side of the membrane. This rise in pressure was tracked over a period of time up to 60 min in the case of gases with low permeability. After enough data were collected, the permeate-side valve was opened, and the gas flux was allowed to reach steady state once again. Sets of data were collected over a period of 4–6 h and the permeability was found to remain constant. Hence, there are no transient effects in the permeability data. To measure the temperature effect on permeability, the module was heated to above ambient temperatures. A J-type thermocouple was inserted into the module through the probe gas line so that it was touching the top surface of the membrane. The minimum variation in this membrane surface temperature during the course of a run was only 2°C. Experiments were performed using helium, hydrogen, oxygen, nitrogen, carbon dioxide, and ethylene. Data sets were collected for at least three different temperatures and the module was gas tight.

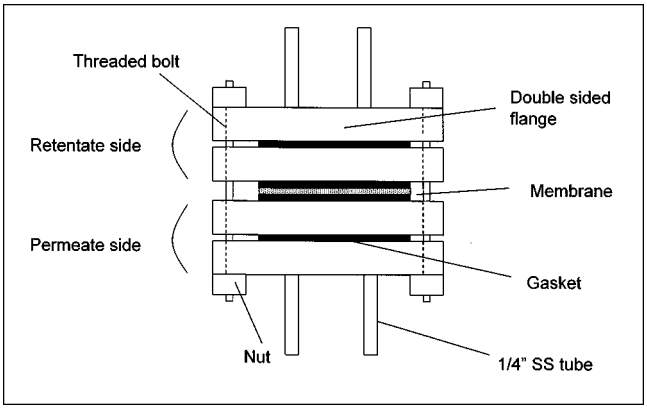

Figure 1. Experimental membrane apparatus.

Molecular size determination

The apparent size of a molecule can vary by as much as 0.5 Å, depending on the method used for its estimation. When correlating permeabilities or transport activation energies to size, such large differences are clearly unacceptable. Of the different values available in the literature, the ones used for the analysis presented here are listed in Table 1. The Lennard-Jones diameters are those based on the 6–12 potential function and derived from viscosity measurements (Reid et al., 1987). The maximum and minimum molecular dimensions were obtained from molecular model measurements using Cerius software (Molecular Simulations Inc.), coupled with estimates of van der Waals' radii (Hirschfelder et al., 1954). The plane of each molecule was aligned with the Cartesian axes and the measurements along the *x*-, *y*-, and *z*-directions were obtained. For example, the measurements for hydrogen along the three axes are *x* and *y* axes = 2.4 Å (the van der Waals' diameter of the hydrogen atom) and the

Table 1. Diameters and Minimum Projected Areas of Probe Molecules Based on Different Potential Functions and Computed van der Waals Radii

Molecule	LJ Diameter*	Min 0**	Min 1**	Max**	Prj. Area Å^2 Min0×Min1
He	2.551	2.55	2.55	2.551	6.50
H_2	2.827	2.40	2.40	3.108	5.76
O_2	3.467	3.04	3.04	4.190	9.24
N_2	3.798	3.10	3.10	4.220	9.61
CO_2	3.941	3.40	3.40	5.432	11.36
C_2H_4	4.163	3.40	4.275	5.464	14.53

*From Reid et al. (1987).
**Calculated from Cerius with van der Waals' diameters from Hirschfelder et al. (1954), except for Helium.

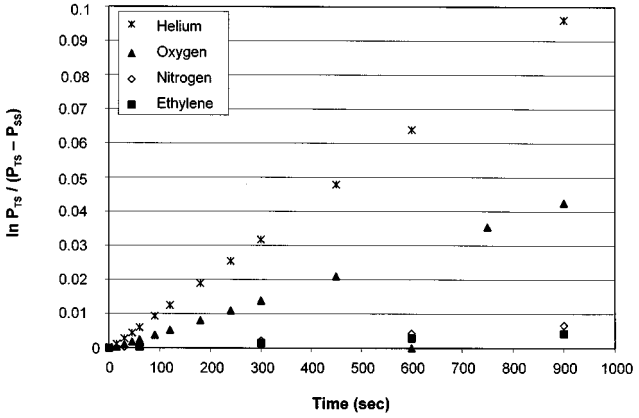

Figure 2. Permeance regression plots for membrane A.

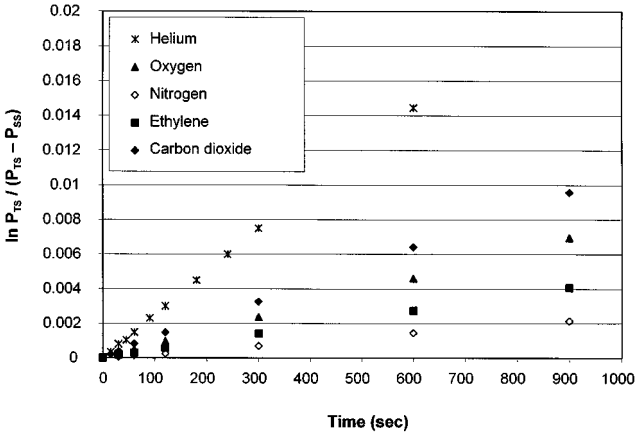

Figure 4. Permeance regression plots for membrane C.

z-axis = 3.1 Å (sum of the bond length of 0.7 Å and the van der Waals' diameter). Similarly, the dimensions of CO_2 are as follows: x and y axes = 3.4 Å (diameter of the carbon atom) and the z-axis = 5.432 Å (sum of the O−O distance and the O atom diameter). The molecular dimensions of ethylene when aligned are x-axis = 3.4 Å (diameter of carbon atom), y-axis = 4.275 Å (H−H distance for atoms attached to the same carbon atom), and z-axis = 4.824 Å (H−H distance between atoms attached in the *cis*- position to different C atoms). However, there is another distance of 5.464 Å between the H atoms in the *trans*- position, which is actually the largest dimension in the molecule. Min0 is the smallest dimension of the molecule, while Min1 is the next smallest, and their product is the projected area.

Results

Rise-time experimental data were analyzed using a simple model developed earlier (Acharya, 1997). The expression obtained by doing a simple mass balance around the membrane is

$$\ln \frac{P_{TS}}{(P_{TS} - P_{SS})} = \frac{ART}{V_{SS}} \frac{P_m}{l} t = \frac{ART}{V_{SS}} \pi t. \qquad (2)$$

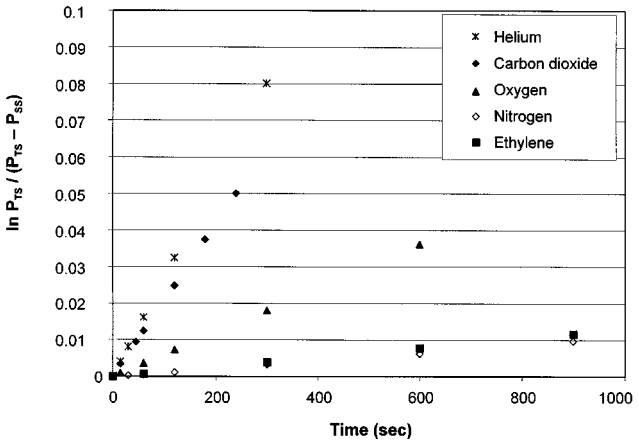

Figure 3. Permeance regression plots for membrane B.

A plot of the lefthand side expression vs. t gives a quantity from which the permeability P_m can be directly obtained. The exact thickness of the membrane layer, however, could not be determined precisely—hence, rather than create ambiguity in the calculations, we choose to focus on the permeance π, which is equal to the permeability divided by the membrane thickness. We also know from independent measurements done by scanning electron microscopy that since the preparation of each membrane followed the same route, the layer thicknesses are very close to being the same.

Figures 2−4 show the straight line fits to data on membranes A through C. The fits for the regression plots all had R-square values of 0.99 and greater, which proves that the simple model is extremely suitable for analyzing the data. The pure component permeances of the probe gases regressed from the data are shown (Figure 5) as a function of the membrane synthesis temperature. The permeances for all gases rose from membrane A to B, but decreased by almost an order of magnitude in membrane C. Pure-component selectivities for pairs of molecules on the three membranes were

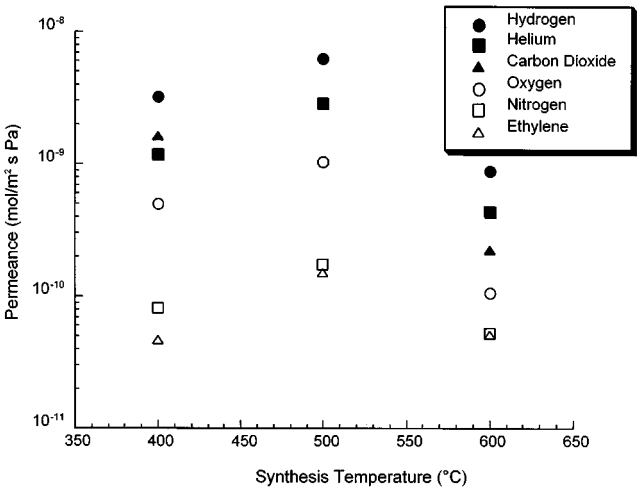

Figure 5. Permeance of probe molecules as a function of membrane synthesis temperature.

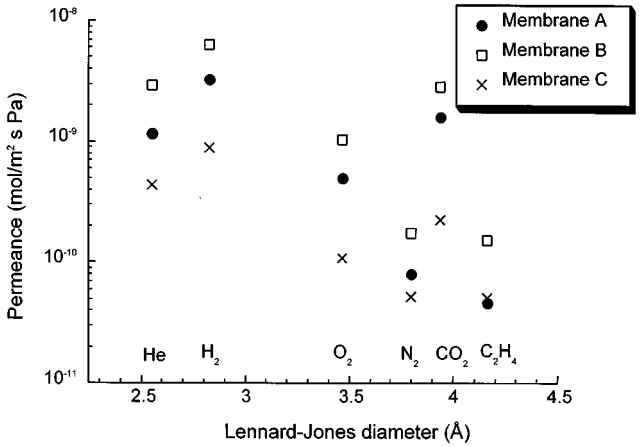

Figure 6. Permeance of probe molecules as a function of Lennard-Jones diameter.

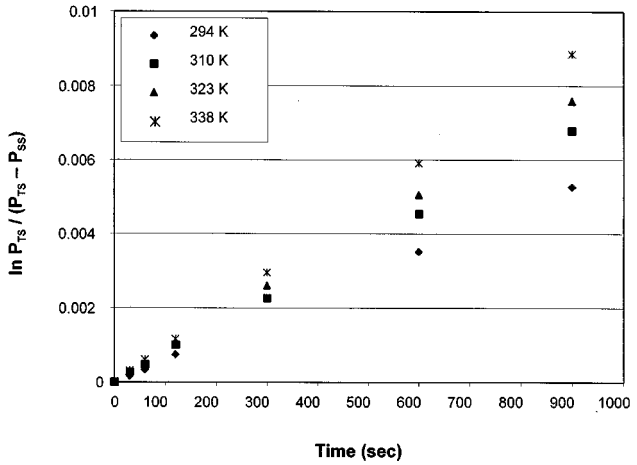

Figure 8. Rise-time data at different temperatures for oxygen.

significantly higher than the corresponding Knudsen selectivity (calculated as the inverse ratio of the square root of molecular weights), which places the transport in the regime of configurational diffusion.

In order to determine the variation of transport properties with molecular size, probe molecule permeances through all three membranes at 294 K were plotted vs. Lennard-Jones diameters (Figure 6). The data appear to be quite scattered, with no clear dependence on size. The same scatter was also observed in plots vs. the minimum and maximum dimensions.

Rise-time data collected at different temperatures were also analyzed using the simple model, and are shown for a few gases in Figure 7–11. The change in the slope of the straight-line fit is an indication of the sensitivity of the permeance to temperature. Thus, in the case of helium, there was very little change in permeance even at 50°C, while for a gas like nitrogen, the change is quite noticeable.

Permeances were again regressed from the data and an Arrhenius expression was used to extract the observed activation energy:

$$\pi = \pi_o e^{(-E_{obs}/RT)}, \tag{3}$$

where E_{obs} is the observed activation energy for permeation and π_o is a constant (Table 2). The maximum error in determining these values was around 0.3 kcal/mol.

The dependence of observed activation energy on size was quite uncorrelated. At first glance, therefore, it seems like the transport properties of these molecules over nanoporous carbon membranes cannot be related to size. It is necessary, therefore, to delve deeper into the mechanism of transport at a molecular level to better understand the reason for the seemingly nonexistent correlation.

Analysis and Model Development

Gas permeation in nanoporous membranes is a process that combines adsorption and transport effects. Permeance is

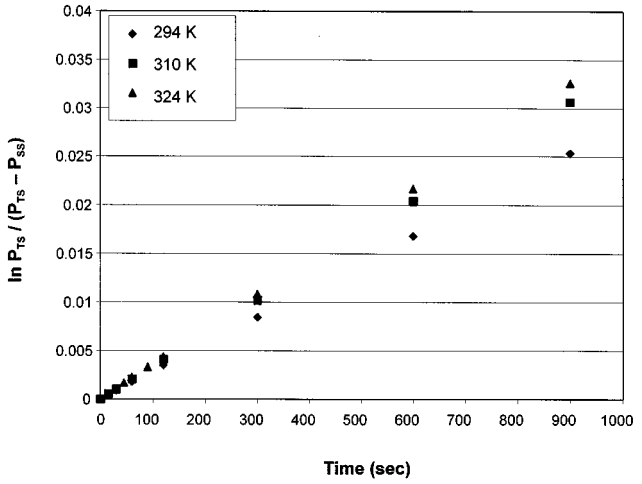

Figure 7. Rise-time data at different temperatures for helium.

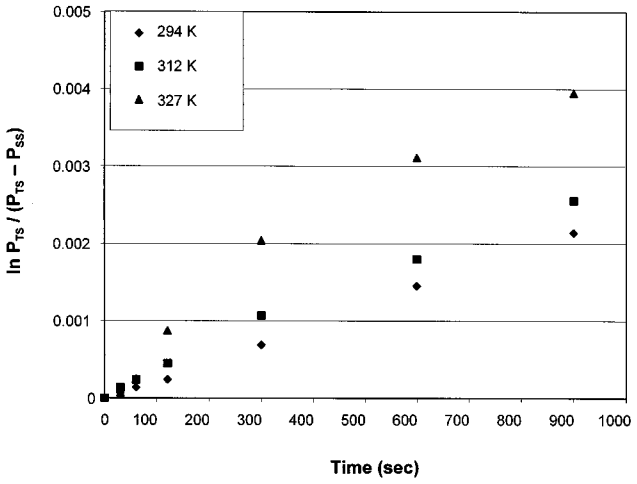

Figure 9. Rise-time data at different temperatures for nitrogen.

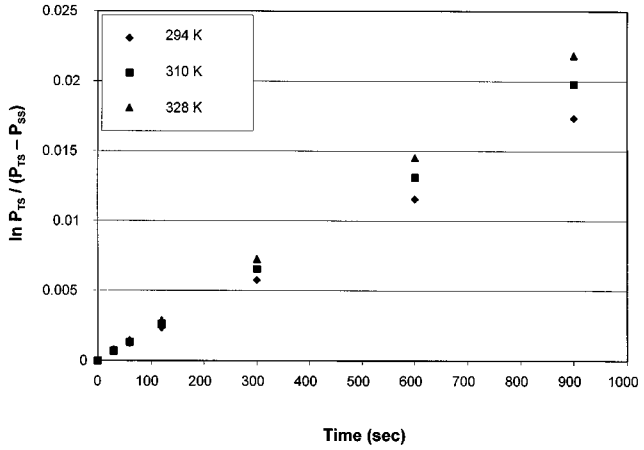

Figure 10. Rise-time data at different temperatures for carbon dioxide.

therefore an extrinsic measure of membrane performance. To obtain more intrinsic information on the transport, the adsorption effect must be handled separately. In order to do so, we write the permeance as the product of the diffusivity and the slope of the isotherm in the region of measurement:

$$\pi = \frac{dC}{dP}\frac{D_{\text{eff}}}{\delta}. \tag{4}$$

In the experimental data, we find little or no pressure dependence in the permeance, which is consistent with our experience with these membranes (Acharya et al. 1997; Shiflett and Foley, 1999). This is not surprising, and is one of the essential features of a membrane that will discriminate primarily on the basis of penetrant size and shape. In this regime of no pressure dependence, therefore, we take the concentration of the gas in the membrane to be given by Henry's law, and the derivative of concentration with pressure is the Henry's law

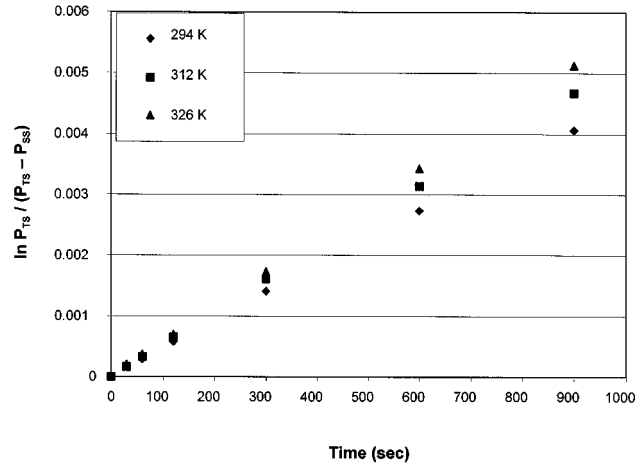

Figure 11. Rise-time data at different temperatures for ethylene.

Table 2. Observed Activation Energies for Molecules on Membranes

Molecule	Memb. A kcal/mol	Memb. B kcal/mol	Memb. C kcal/mol
Helium	0.94	0.81	1.36
Oxygen	0.55	3.29	1.94
Nitrogen	2.98	5.21	3.75
Carbon dioxide	0.47	1.29	0.9
Ethylene	5.84	4.7	1.01

constant (K):

$$C = C_{\text{sat}} KP$$

$$dC/dP = C_{\text{sat}} K. \tag{5}$$

Since the permeance lacks pressure dependence, and so too does K, it is clear that D_{eff} is also pressure independent.

We also know that the effective diffusivity depends on the porosity ϵ and the tortuosity τ of the medium, which are not intrinsic to the transport. Therefore, Eq. 4 can be rewritten as

$$\pi = \frac{\epsilon C_{\text{sat}} KD}{\tau\delta}. \tag{6}$$

The tortuosity τ is often taken as $1/\epsilon$ (Weisz and Schwartz, 1962). The porosity is related to the density of the nanoporous carbon by the following equation:

$$\epsilon = \frac{\rho_{gr} - \rho_{\text{net}}}{\rho_{gr}} \tag{7}$$

where ρ_{gr} is the density of graphite and ρ_{net} is the density of the membrane carbon. The relationship between the density of NPC and preparation temperature has been reported previously (Kane et al., 1996; Acharya et al., 1999). We use this relationship to derive the NPC membrane densities, and hence their void fractions. In turn K can be written in terms of the van't Hoff relation as

$$K = K_0 e^{(q_{\text{iso}}/RT)}, \tag{8}$$

where q_{iso} is the isosteric heat of adsorption of the molecule and K_0 is a temperature independent constant. The isosteric heats for adsorption onto nanoporous carbon were assumed from literature values for other materials such as activated carbons and zeolites (Table 3). Due to the lack of the nanoporous carbons that we were using, we found it necessary to use these other data.

According to transition state theory, nanopore transport involves the movement of a molecule from a state of relative equilibrium to an intermediate, constrained state of higher energy. The expression for diffusivity of a molecule is given by

$$D = \lambda^2 \frac{k_B T}{h} e^{\Delta S^{\neq}/Re - \Delta H^{\neq}/RT}, \tag{9}$$

Table 3. Isosteric Heats of Adsorption of Probe Molecules

Molecule	Isosteric Heat of Adsorption (kcal/mol)
Helium	~ 0
Oxygen	3.14*
Nitrogen	2.07**
Carbon Dioxide	5.66†
Ethylene	6.46†

*Value for zeolite 10×.
**Average of values measured for zeolite 10× and activated carbon.
†Average of values measured for activated carbon and CMS.

where λ is the jump distance between two equilibrium states of the molecule, k_B is the Boltzmann constant, h is Planck's constant, and $\Delta S^{\neq}$ and $\Delta H^{\neq}$ are, respectively, the difference in entropy and enthalpy between the transition and the normal state of the molecule. The term $\Delta S^{\neq}$ takes into account the sizes of the molecule and the pore, while $\Delta H^{\neq}$ is based primarily on the energetics of pore–molecule interactions. Combining each of the equations, the expression for permeance now becomes:

$$\pi = \frac{K_0 C_{\text{sat}} \lambda^2 k_B T \epsilon}{\tau \delta h} e^{(q_{\text{iso}}/RT)} e^{(\Delta S^{\neq}/R)} e^{(-\Delta H^{\neq}/RT)}. \quad (10)$$

We can now define an intrinsic permeance π by rearranging Eq. 8 to give:

$$\pi' = \frac{\pi}{\epsilon^2 e^{(q_{\text{iso}}/RT)}} = \frac{K_0 C_{\text{sat}} \lambda^2 k_B T}{h \delta} e^{(-\Delta G^{\neq}/RT)}. \quad (11)$$

The intrinsic permeance is independent of membrane porosity as well as differences in adsorption strength between molecules. The free-energy values for the different molecules are obtained by plotting the log of the lefthand side of Eq. 11 vs. $1/T$. The slope of the straight line fit is $\Delta G^{\neq}/R$ and the intercept is $K_0 C_{\text{sat}} \lambda^2 k_B T/h$. The plots for the different molecules are shown in Figure 12, and the values for the free energies of transition are shown in Table 4.

Table 4. Transition-State Free-Energy Change for Molecules on Membranes

Molecule	Memb. A kcal/mol	Memb. B kcal/mol	Memb. C kcal/mol
Helium	0.98	0.81	1.36
Oxygen	3.66	6.48	5.13
Nitrogen	5.07	7.3	5.83
Carbon dioxide	6.15	6.97	6.6
Ethylene	12.34	11.15	7.5

Size Dependence of Intrinsic Permeance

The intrinsic permeances of all the probe molecules are plotted vs. their Lennard-Jones diameters in Figure 13. The intrinsic permeance of carbon dioxide is lower than that of oxygen and nitrogen, which is consistent with the simple transport model, but that of hydrogen is still higher than that of helium. The plot of intrinsic permeances vs. the minimum projected areas is shown in Figure 14. The data are now well correlated with size. Referring to our discussion earlier in the text, the dimensions for carbon dioxide, for example, are 3.4 Å and 3.4 Å, and for ethylene, they are 3.4 Å and 4.275 Å. The definition of minimum projected area therefore differentiates between ethylene and carbon dioxide, which have the same minimum dimension of 3.4 Å, but their next largest dimensions are different. It also explains the data for hydrogen, whose smallest dimensions are both 2.4 Å, and hence is smaller than the 2.551-Å helium molecule. Therefore, in correlating intrinsic permeances to size, the minimum projected area of the molecule provides the best agreement with the simple transport model. Fitting an exponential curve to the plot, the variation in permeance with projected area is found to be remarkably similar for each of the membranes:

$$\pi' = Ce^{(-1.724 d_{ar}^2)}, \quad (12)$$

where C is a constant and d_{ar} is the equivalent diameter of the molecule, defined as the square root of the minimum projected area of the molecule.

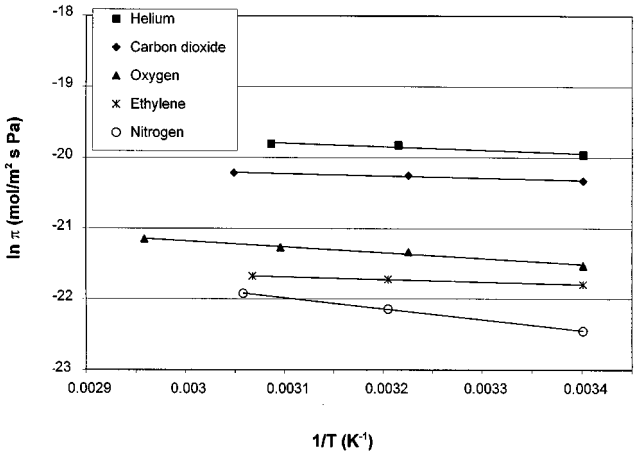

Figure 12. Regression of activation energies from permeance data on membrane C.

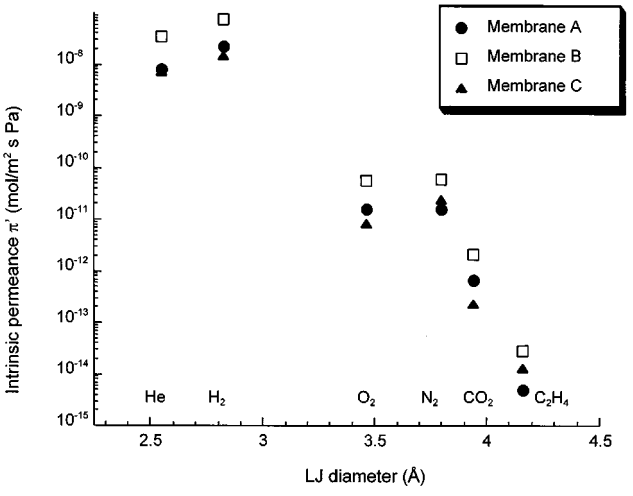

Figure 13. Intrinsic permeances of probe molecules at 294 K vs. Lennard-Jones diameter.

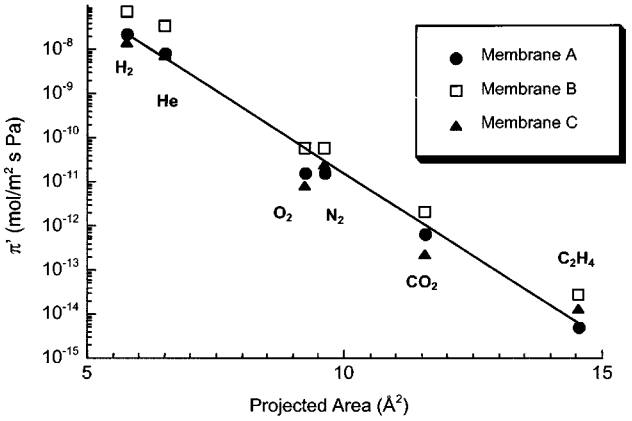

Figure 14. Intrinsic permeances of probe molecules at 294 K vs. minimum projected area.

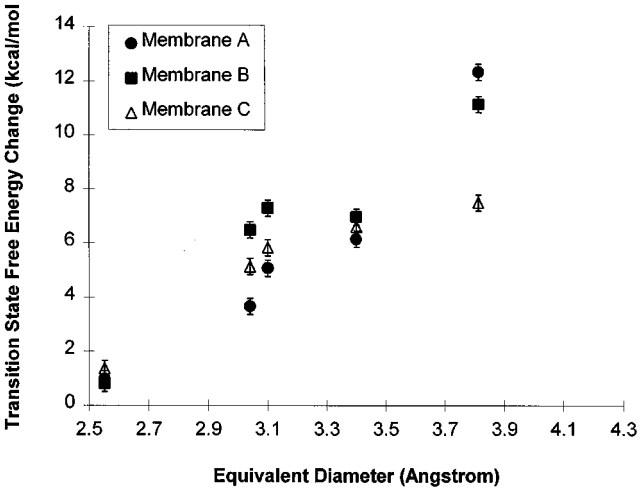

Figure 15. Transition-state free-energy change of probe molecules as a function of their equivalent diameter over nanoporous carbon membranes.

The result of Eq. 12 is not unexpected—the intrinsic permeance should be primarily size dependent, since membrane porosity and molecular adsorption effects have been eliminated. The presence of K_0, the preexponential term from the van't Hoff relationship for the Henry's law constant for each molecule, does not affect the fit to the data. Comparing the exponential terms in Eq. 12 and Eq. 11, we see that the free energy should vary linearly with the projected area. This dependence is discussed in the following section.

Size Dependence of Free-Energy Change

The transition-state free-energy change $\Delta G^{\neq}$ was obtained for all molecules from Eq. 11 and are listed in Table 4. This free-energy change is simply equal to the intrinsic activation energy for diffusion. It is apparent, in comparison to the observed activation energies, that the presence of the adsorption term causes a large reduction in the intrinsic activation energy for strongly adsorbing molecules such as carbon dioxide and ethylene. The variation in free energy with projected area is shown in Figure 15. The free energy tends to increase with projected area, as Eq. 12 would predict; however, the trend is not quite linear in all cases. In fact, in membrane *C*, the free energies almost level off at higher values of the projected area, that is, for larger molecules.

The free energy consists of an entropic and enthalpic component, both of which have a dependence on size. The entropic component is easier to calculate since it depends purely on the dimensions of the molecule and the pore. We present below a simple model to calculate the entropy change of a molecule in going to the transition state.

Hard-sphere entropic model

The picture of molecular transport inside a nanopore that we have developed so far consists of a molecule moving in the gas phase through an open region, referred to as a "gallery," and then encountering a constriction where it has to go into a transition state to overcome the energy barrier. While the molecule is able to move around relatively freely in the gallery, it is limited in the number of available configurations it can attain in the transition state. This restriction represents a loss in entropy of the molecule, which can be calculated from the volume as

$$\Delta S^{\neq} = R \ln \frac{V^{\neq}}{V_f}, \tag{13}$$

where V is the volume available to the molecule in the transition state and V_f is the free volume occupied by the molecule in the gallery.

Figure 16 shows a molecule in a gallery approaching a constriction. To simplify the problem, we consider the transport in only two dimensions. The molecule is assumed to be a diatomic hard sphere with radius r_m and the constriction has a radius r_p. In the simplest case, the molecule approaches along the axis of the pore. The loss in free volume is then equal to the two slices of the volume of revolution that are cut off by the pore edges, as shown in Figure 16a. The expression for the entropy change is then given by

$$\Delta S^{\neq} = R \ln \left[\frac{1}{2} \left(\frac{3r_p}{r_m} - \frac{r_p^3}{r_m^3} \right) \right]. \tag{14}$$

This expression depends solely on the ratio of molecular to pore size. One of the limitations of this is that a molecule smaller than the pore constriction should not experience any entropic barriers whatsover. This is not likely, since a molecule cannot be expected to follow a straight-line trajectory into the constriction. It is more likely that the molecule approaches the constriction at an angle θ and an offset from the axis, as shown in Figure 16b. So the total entropy change comes from not only molecular-size effects, but also from the variation in approach of the molecule to the constriction:

$$S_{\text{total}} = S(r_p, r_m) + S(\theta) + S(x). \tag{15}$$

If the volume of revolution of the molecule is projected onto the constriction, then there is only a small portion (between

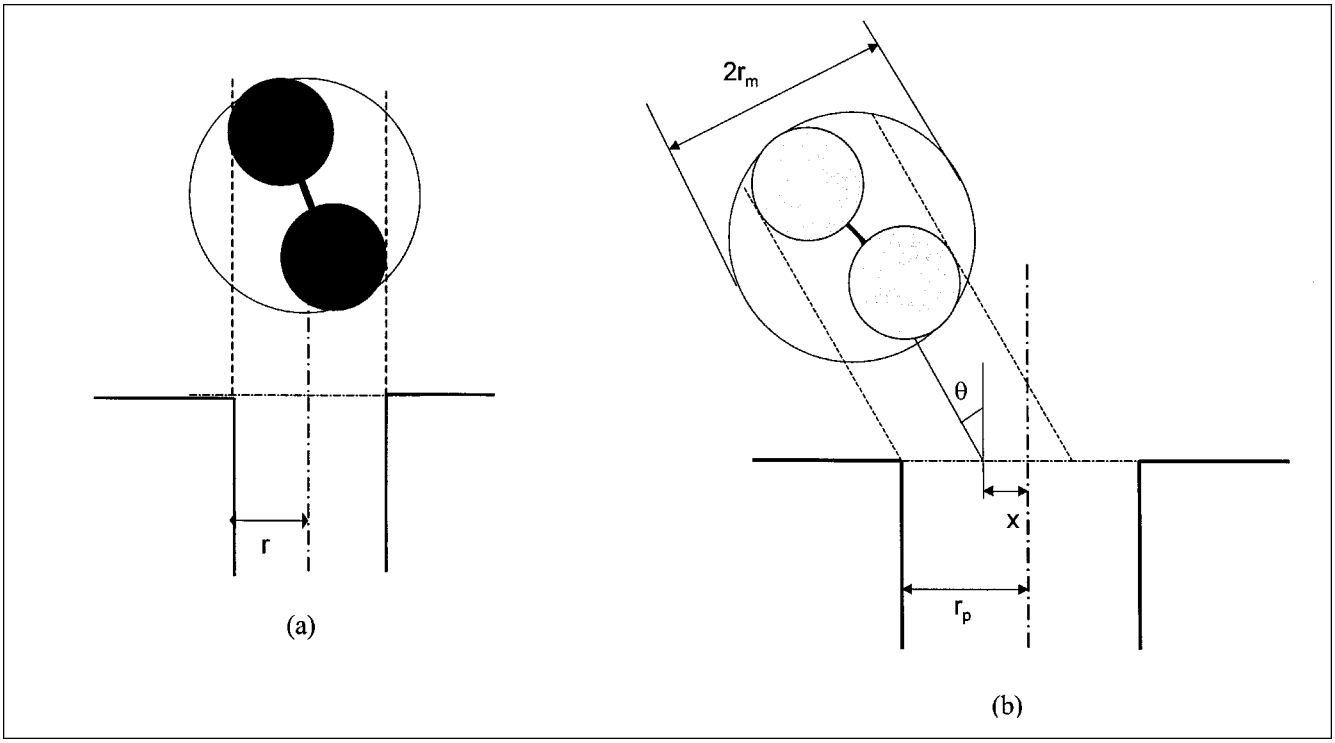

Figure 16. Model of diatomic molecule approaching slit-shaped pore mouth.

Only configurations of the molecule within the dashed lines can fit into the pore if the center of mass is fixed.

the dashed lines) that can fit within the constriction (the center of mass of the molecule is fixed). This volume, which is the total volume of revolution minus the two frusta of the sphere, represents the volume of the transition state of the molecule and can be calculated as

$$V^{\neq} = \frac{\pi}{3}(r_p - x)\cos\theta\left[6r_m^2 - 2(r_p - x)^2\cos^2\theta\right] \quad (16)$$

This is the volume occupied by the sphere of revolution of the molecule at the constriction. Averaging this expression over the entire range of possible approach trajectory angles for the molecule (x ranging from 0 to r_P and θ ranging from 0 to $\pi/2$), we get

$$V^{\neq} = \frac{2r_m^2 r_p}{9}\left(9 - \left\{\frac{r_p}{r_m}\right\}^2\right). \quad (17)$$

The change in entropy on going from free space into the constriction is

$$\Delta S^{\neq} = R\ln\frac{V^{\neq}}{V_f}, \quad (18)$$

where V_f is the volume of the sphere in free space ($= 4/3\pi r_m^3$). Combining Eqs. 17 and 18, we get

$$\Delta S^{\neq} = R\ln\left(\frac{1}{6\pi}\frac{r_p}{r_m}\left\{9 - \left(\frac{r_p}{r_m}\right)^2\right\}\right). \quad (19)$$

This expression is slightly different from the one for axial approach of the molecule in Eq. 13. For one thing, molecules that are smaller than the pore size also have an entropic barrier to face. This term is evaluated over the entire pore-size distribution to obtain the average entropic change as

$$\Delta\bar{S}^{\neq}(r_m) = \frac{\int_0^{\infty}\Delta S^{\neq}(r_p, r_m) f(r_p)\, dr_p}{\int_0^{\infty} f(r_p)\, dr_p}. \quad (20)$$

The average transition-state entropic changes for the probe molecules were computed by numerical integration, and are listed in Table 5. The sizes of the molecules used were the equivalent diameter, defined as the square root of their respective minimum projected areas. A normal distribution with a mean of 4 Å and standard deviation of 0.5 Å was used as the pore-size distribution of all the membranes. Previous data (Mariwala and Foley, 1994) has shown that this assumption is correct.

The enthalpic change is then calculated from the equation:

$$\Delta H^{\neq} = \Delta G^{\neq} + T\Delta\bar{S}^{\neq}. \quad (21)$$

Figure 17 shows the enthalpy change data vs. projected area. The straight line is the best fit to this data. The values for the enthalpy of transition vary from just above zero to almost 12 kcal/mol. These numbers and their range are in good agreement with what we expect to find for the NPC based on other studies that have been done on similar materials, either in

Table 5. Average Transition-State Entropic Change Calculated from Simple Entropic Model for all Molecules

Molecule	$\Delta S^{\neq}$ cal/mol·K
Helium	−1.246
Oxygen	−1.375
Nitrogen	−1.395
Carbon dioxide	−1.501
Ethylene	−1.654

bulk or membrane form. There is, however, no absolute set of numbers for this transition energy to which these values can be compared. We can compare the numbers to the potential energies of each molecule confined to a slitlike pore. This is done in the next section.

Mean Field Potential Energy Comparison

The pore geometry we have modeled so far is that of a narrow slit with fixed spacing. For such a system, a comparison with the potential energy exerted by two parallel graphene sheets on a molecule confined to the space between them, may be computed using a mean field potential model. For this purpose, we chose the MFP derived by Everett and Powl (1976):

$$\phi(z) = \frac{N_a A_a}{2\sigma^4}\left[-\left(\frac{\sigma}{z}\right)^4 + \left(\frac{\sigma}{z}\right)^{10} - \left(\frac{\sigma}{l-z}\right)^4 + \left(\frac{\sigma}{l-z}\right)^{10}\right] \tag{22}$$

Here N_a is the molecular density of the adsorbent (in this case, carbon), z is the position of the molecule between the layers, σ is a variation related to the diameters of the probe molecule and carbon atom, and l is the slit width. The term outside the parentheses is the well depth ϕ_0 of the potential function between the probe molecule and the pore. Table 6 lists the various parameters for the probe molecules. The Kirkwood−Muller approximation was used to determine A_a, and the value of N_a for carbon was taken from the work by Horvath and Kawazoe (1983).

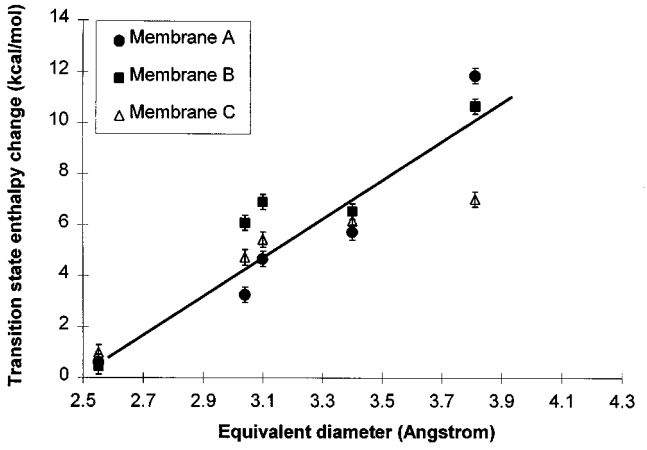

Figure 17. Transition-state enthalpy change for probe molecules versus equivalent diameter.

Table 6. Polarizability, Magnetic Susceptibility, and Well Depth for Probe Molecules and Adsorbent Atom*

Molecule	Polarizability ($\times 10^{25}$ cm^3)	Magnetic Susceptibility ($\times 10^{30}$ cm^3)	Well Depth (kcal)
Helium	2.049	3.121	0.398
Oxygen	15.81	5726	3.664
Nitrogen	17.4	20	2.106
Carbon dioxide	29.11	34.86	2.997
Ethylene	42.52	25.4	2.387
Carbon	10.2	9.96	—

*Data obtained from the *CRC Handbook of Chemistry and Physics.*

The potential energies of all the molecules we studied were calculated using Eq. 19 for pores of diameter 3−6 Å. The minimum energy state for each molecule was at the center of the pore. The enthalpy change in going to the transition state $\Delta H^{\neq}$ was taken as equal to the potential energy of the molecule in its transition state, and the equivalent diameter of each molecule (square root of the projected area) was used for the calculation. Thus, we make the assumption that the molecules are transported in the gas phase within the pore. Since we have removed the effect of adsorption, we feel that this assumption is reasonable. Figure 18 shows the fit of the Everett−Powl model to the enthalpy change data for different pore diameters. The first thing one notices is that the EP model also predicts a nearly straight-line dependence of energy on the projected area. Using no other adjustable parameters, the best fit to the data is obtained when the constriction spacing was 4.6 ± 0.1 Å. Recall that we had used a mean constriction size of 4.0 Å for the entropy calculation. The fact that the EP-MFP comes as close as it does to the enthalpies of transition that we have computed suggests that the values are reasoanble. The slope of the potential function prediction is less than that of the best-fit straight line drawn through the data points. This may be due to the fact that we have considered only one pore size. However, the fact that the

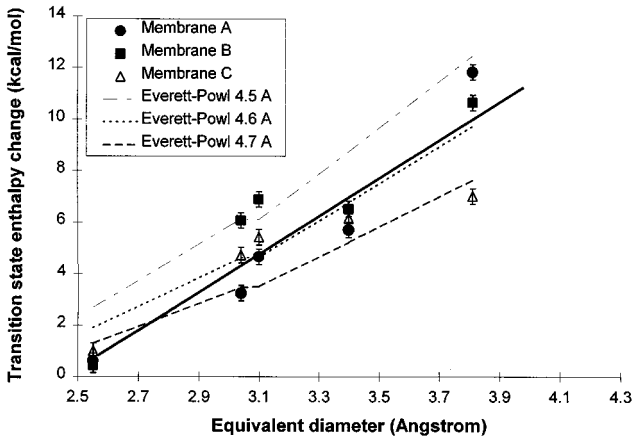

Figure 18. Everett-Powl model prediction using equivalent diameter for the transition-state enthalpy change.

The linear best fit to the data is also plotted.

best fit to the data should occur at a mean pore size of 4.6 Å is remarkable, since this value is so close to the mean value that we had assumed for the pore constriction size in the entropy computation. Furthermore, that NPC membranes such as these, which do separate oxygen from nitrogen on the basis of the kinetics of transport, should have an apparent pore size of close to 4.0 Å, is expected and is completely consistent with previous work. From the literature on this separation, the consensus is that the bulk NPC materials used in pressure-swing adsorptive separation of air for the recovery of nitrogen have a pore size of approximately 4.0 Å or less.

On the other hand, we see that the EP potential function cannot predict the observed difference in the activation enthalpy between oxygen and nitrogen, but rather predicts similar values for the two. Under these circumstances, it is difficult to understand how separation factors between these two molecules well above the Knudsen limit are obtained. We already know that the entropic barrier based on our hard sphere model is nearly the same for both molecules. It is possible that the EP model, like all purely dispersive potentials, fails to include the effect of an electrostatic attractive potential within the pore constriction, which favors entry of the oxygen molecule. The large difference in magnetic susceptibility between the two molecules could be the cause of such an attractive potential. Accordingly, the selectivity for oxygen would not arise from a larger entropic barrier at the pore constriction for nitrogen, but rather from a slightly less repulsive and, hence, lower enthalpic barrier for the transit of oxygen vs. nitrogen. Further work is underway to define and develop this hypothesis.

Summary

The permeances measured herein were found to correlate well with the minimum projected area of the molecules rather than with any single dimension of volume. The experimental transition-state free-energy changes, $\Delta G^{\neq}$, and the entropies, $\Delta S^{\neq}$, computed from a simple hard-sphere model, were used to determine the transition-state enthalpies, $\Delta H^{\neq}$. Within the limits of experimental error, $\Delta H^{\neq}$ varied linearly with the equivalent molecular diameter. The Everett–Powl potential energy function, commonly used in adsorption modeling in NPC, gave a remarkably good fit to the enthalpies. Only one adjustable parameter, namely, the average pore size was used to obtain this fit. These results suggest that the enthalpy of transition is as important, if not more important, than the entropy of transition in determining the size and shape effects displayed by the diffusion of small molecules in NPC membranes.

Notation

A = membrane cross-sectional area, cm^2
A_a = Kirkwood–Muller potential factor, J·cm
C_{sat} = permeate saturation concentration in membrane, mol/cm^3
C_o = constant, mol/cm^2 s Pa
D_{eff} = effective diffusivity, cm^2/s
$E_{a,diff}$ = activation barrier for diffusion, kcal/mol
$f(r_p)$ = pore size distribution
K_o = preexponential factor for Henry's constant, 1/Pa
P_{TS} = pressure shell (top, feed) side of membrane, Pa
P_{SS} = pressure shell (bottom, permeate) side of membrane, Pa
R = ideal gas constant, cm^3 Pa/K·mol
T = absolute temperature, K
t = time, s
V_{SS} = volume shell side, cm^3
δ = membrane thickness, cm
π_o = permeance pre-exponential factor, mol/cm^2·s·Pa

Literature Cited

Acharya, M., and H. C. Foley, "Spray Coating of Nanoporous Carbon Membranes for Air Separation," *J. Memb. Sci.*, **161**, 1 (1999).

Acharya, M., "Engineering Design and Theoretical Analysis of Nanoporous Carbon Membranes for Gas Separation," PhD Thesis, Univ. of Delaware, Newark (1999).

Acharya, M., B. A. Raich, H. C. Foley, M. P. Harold, and J. J. Lerou, "Metal Supported Carbogenic Molecular Sieve Membranes—Synthesis and Applications," *Ind. Eng. Chem. Res.*, **8**, 2924 (1997).

Acharya, M., M. S. Strano, J. P. Mathews, S. J. L. Billinge, S. Subramoney, and H. C. Foley, "Simulation of Nanoporous Carbons: A Chemically Constrained Structure," *Philos. Mag. B.*, **79**, 1499 (1999).

Armor, J. N., "Molecular Sieves for Air Separation," *Adv. Chem.*, **245**, 321 (1995).

Braymer, T. A., C. G. Coe, T. S. Farris, T. R. Gaffney, J. M. Schork, and J. N. Armor," *Granular Carbon Molecular-Sieves," Carbon*, **32**, 445 (1995).

Cabrera, A. L., J. E. Zehner, C. G. Coe, T. R. Gaffney, T. S. Farris, and J. N. Armor, "Preparation of Carbon Molecular Sieves I Two-Step Hydrocarbon Deposition with a Single Hydrocarbon," *Carbon*, **31**, 969 (1993).

Chihara, K., M. Suzuki, and K. Kawazoe, "Interpretation for the Micropore Diffusivities of Gases in Molecular-Sieving Carbon," *J. Colloid. Interface Sci.*, **64**, 584 (1978a).

Chihara, K., M. Suzuki, and K. Kawazoe, "Adsorption Rate on Molecular Sieving Carbon by Chromatography," *AIChE J.*, **24**, 237 (1978b).

CRC Handbook of Chemistry and Physics, 71st ed., CRC Press, Boca Raton, FL (1990).

Everett, D. H., and J. C. Powl, "Adsorption in Slit-Like Cylindrical Micropores in the Henry's Law Region," *J. Chem. Soc., Faraday Trans. I*, **72**, 619 (1976).

Ford, D. M., and E. D. Glandt, "Steric Hindrance at the Entrance to Small Pores," *J. Membr. Sci.*, **107**, 47 (1995).

Gaffney, T. R., "Porous Solids for Air Separation," *Curr. Opin. Solid State Mat. Sci.*, **1**, 69 (1996).

Glasstone, S., *The Theory of Rate Processes: The Kinetics of Chemical Reactions, Viscosity, Diffusion and Electrochemical Phenomena*, McGraw-Hill, New York (1941).

Hirschfelder, J. O., C. F. Curtiss, and R. B. Bird, *Molecular Theory of Gases and Liquids*, Wiley, New York (1954).

Horvath, G., and K. Kawazoe, "Method of the Calculation of Effective Pore Size Distribution in Molecular Sieve Carbon," *J. Chem. Eng. Jpn.*, **16**, 471 (1983).

Juntgen, H., K. Knoblauch, and K. Harder, "Carbon Molecular Sieves: Production from Coal and Application in Air Separation," *Fuel*, **60**, 817 (1981).

Kane, M. S., J. F. Goellner, H. C. Foley, R. DiFrancesco, S. J. L. Billinge, and L. F. Allard, "Symmetry Breaking in Nanostructure Development of Carbogenic Molecular Sieves: Effects of Morphological Pattern Formation on Oxygen and Nitrogen Transport," *Chem. Mat.*, **8**, 2159 (1996).

Kasakabe, K., M. Yamamoto, and S. Morooka, "Gas Permeation and Micropore Structure of Carbon Molecular Sieving Membranes Modified by Oxidation," *J. Membr. Sci.*, **149**, 59 (1998).

Kawazoe, K., M. Suzuki, and K. Chihara, "Concentration-Dependence of Micropore Diffusivities: Diffusion of Propylene in Molecular Sieving Carbon," *J. Chem. Eng. Jpn.*, **11**, 153 (1978).

Kawazoe, K., M. Suzuki, and K. Chihara, "Chromatographic Study of Diffusion in Molecular Sieving Carbon," *J. Chem. Eng. Jpn.*, **7**, 151 (1974).

La Cava, A. I., V. A. Koss, and D. Wickens, "Non-Fickian Adsorption Rate Behavior of Some Carbon Molecular Sieves," *Gas Sep. Purif.*, **3**, 180 (1989).

Lamond, T. G., J. E. Metcalfe, III, and P. L. Walker, Jr., ''Molecular Sieve Properties of Saran-Type Carbons,'' *Carbon*, **3**, 59 (1965).
Mariwala, R. K., and H. C. Foley, ''Evolution of Ultramicroporous Adsorptive Structure in Poly(furfuryl alcohol)-Derived Carbogenic Molecular Sieves,'' *Ind. Eng. Chem. Res.*, **33**, 607 (1994).
Moyer, J. D., T. R. Gaffney, J. N. Armor, and C. G. Goe, ''Defining Effective Microporosity in Carbon Molecular Sieves,'' *Microporous Mat.*, **2**, 229 (1994).
Parrillo, D. J., C. Thaeron, and S. Sircar, ''Separation of Bulk Hydrogen Sulfide-Hydrogen Mixtures by Selective Surface Flow Membrane,'' *AIChE J.*, **43**, 2239 (1997).
Petkov, V., R. G. DiFrancesco, S. J. L. Billinge, M. Acharya, and H. C. Foley, ''Local Structure of Nanoporous Carbons,'' *Philos. Mag. B.*, **79**, 1519 (1999).
O'Brien, K. C., W. J. Koros, T. A. Barbari, and E. S. Sanders, ''A New Technique for the Measurement of Multicomponent Gas Transport Through Polymeric Films,'' *J. Memb. Sci.*, **29**, 229 (1986).
Rao, M. B., S. Sircar, and T. C. Golden, ''Gas Separation by Adsorbent Membranes,'' U.S. Patent No. 5,104,425 (1992).
Rao, M. B., and S. Sircar, ''Nanoporous Carbon Membranes for Separation of Gas Mixtures by Surface Selective Flow,'' *J. Memb. Sci.*, **85**, 253 (1993).
Rao, M. B., and S. Sircar, ''Performance and Pore Characterization of Nanoporous Carbon Membranes for Gas Separation,'' *J. Memb. Sci.*, **110**, 109 (1996).
Reid, R. C., J. M. Prausnitz, and B. E. Poling, *Properties of Gases and Liquids*, McGraw-Hill, New York (1987).
Ruthven, D. M., *Principles of Adsorption and Adsorption Processes*, Wiley, New York (1984).
Shelekhin, A. B., A. G Dixon, and Y. H. Ma, ''Theory of Diffusion and Permeation in Inorganic Molecular-Sieve Membranes,'' *AIChE J.*, **41**, 58 (1995).
Shiflett, M. B., and H. C. Foley, ''Ultrasonic Deposition of High-Selectivity Nanoporous Carbon Membranes,'' *Science*, **285**, 1902 (1999).
Singh, A., and W. J. Koros, ''Significance of Entropic Selectivity for Advanced Gas Separation,'' *Ind. Eng. Chem. Res.*, **35**, 1231 (1996).
Suzuki, M., *Adsorption Engineering*, Elsevier, Amsterdam (1990).
Verma, S. K., and P. L. Walker, Jr., ''Preparation of Carbon Molecular Seives by Propylene Pyrolysis over Microporous Carbons,'' *Carbon*, **30**, 829 (1992).
Walker, P. L., Jr., L. G. Austin, and S. P. Nandi, ''Activated Diffusion of Gases in Molecular-Sieve Materials,'' *Chemistry and Physics of Carbon*, P. L. Walker, Jr., ed., Dekker, New York (1965).
Weisz, P. B., and A. B. Schwartz, ''Diffusivity of Porous Oxide Gel-Derived Catalyst Particles,'' *J. Catal.*, **1**, 399 (1962).
Yang, R. T., *Gas Separation by Adsorption Processes*, Butterworth, Boston (1987).

Manuscript received Feb. 18, 1999, and revision received Dec. 1999.